

Performance Analysis of a Single-Diode Photovoltaic Model Based on a Thevenin's Equivalent Circuit

Ammar Al-Gizi^{1*} , Abbas Hussien Miry¹ , Hussein M. Hathal¹ , Aurelian Craciunescu²

¹Electrical Engineering Department, College of Engineering, Mustansiriyah University, Baghdad, Iraq

²Electrical Engineering Faculty, University POLITEHNICA of Bucharest, Bucharest, Romania

*Email: ammar.ghalib@uomustansiriyah.edu.iq

Article Info

Received 13/06/2024

Revised 24/03/2025

Accepted 17/05/2025

Abstract

This article proposes a linear Thevenin's equivalent circuit for a single-diode model. The Thevenin's equivalent circuit is derived based on the piecewise linearization for the nonlinear characteristic of the diode. To validate the accuracy and efficiency of the proposed Thevenin approximation, a photovoltaic module's current-voltage and power-voltage characteristics are evaluated and compared with the characteristics of the original model. Meanwhile, an error of the proposed approximation is also calculated under different values of irradiance and temperature. The operating conditions are classified into three scenarios: standard technical condition (irradiance=1000 W/m², temperature=25 °C), (irradiance=400 W/m², temperature=25 °C), and (irradiance=1000 W/m², temperature=50 °C). Primary results show encouraging outputs and reliability of the proposed model. It is obvious from the simulation results that the linearization technique can successfully emulate the characteristics of the original nonlinear single-diode model. The peak values of the error are 7.37%, 9.51%, and 6.79% at the different suggested scenarios, respectively. Subsequently, the proposed Thevenin equivalent circuit can be successfully used to study the performance of a photovoltaic system under different operating conditions, avoiding the complicated numerical solutions for nonlinear equations of the original photovoltaic model.

Keywords: Current-Voltage characteristics; Piecewise linearization; Power-Voltage characteristics; Single-diode photovoltaic model; Thevenin equivalent circuit

1. Introduction

Two major crises have affected the world in recent years. The first is COVID-19, which caused disruptions in the management and supply network for energy [1]. The second, the conflict between Russia and Ukraine, impacted global energy policy, forcing several countries to embrace more environmentally friendly energy practices [2]. Hence, the necessity of all sources of renewable energy increases as solar, wind, waves, etc., increase. There is a worldwide concern about photovoltaic (PV) systems. Photovoltaics provide an enticing substitute: noiseless, flexible, and pollution-free [3]-[5].

Utilizing effective PV models is essential for achieving the benefits outlined above. Accordingly, modeling of the essential photosystems, such as the PV source, converter, maximum power point tracking (MPPT) controller, etc., must first be generated for performance analysis of the PV system by using a simulator like MATLAB. The PV source, a cell, module, or

array, is the most important part of the PV system. It works as an input to the other parts of the PV system [6].

The literature develops several circuit-based models to simulate the operation of PV sources. The two well-known single-diode and two-diode equivalent circuit models present the base for most of them [7]-[14].

A single-diode PV model, consisting of the current source, a diode, and resistances, is successfully used to model cells and study their characteristics [9]-[13]. Due to the diode's nonlinear characteristic, the PV source exhibits nonlinear current-voltage (*I-V*) and power-voltage (*P-V*) characteristics. Consequently, examining PV characteristics based on the single-diode is complicated and needs a numerical iterative method to solve the nonlinear equations [15]. The Thevenin theorem is invalid because it is tough to derive the PV *I-V* relationship via Ohm's law. Thevenin circuit is a linear circuit consisting of a one voltage source named "Thevenin voltage" (V_{th}) and a single series resistance named "Thevenin resistance" (R_{th}) [16].

This article proposes approximating the diode's nonlinear function $I_d(V_d)$ by a collection of linear functions using the linearization process to transfer the typical PV single-diode equivalent circuit into a simpler one, the Thevenin equivalent circuit. The performance of the proposed model is analyzed using the MATLAB program under different operating conditions. The performance analysis results are compared with the single diode's characteristics to verify the accuracy of the proposed model.

Section 2 of the article explains a piecewise method for the linearization [17]-[18]. Thevenin's equivalent PV circuit follows it. Section 3 presents the proposed model's I-V and P-V characteristics. Section 4 demonstrates the simulation results based on the original and the proposed PV models under different operating conditions. In contrast, Section 5 illustrates notable conclusions.

2. Thevenin Equivalent of PV Model

To derive a Thevenin's equivalent circuit, the original PV single-diode model must first be linearized. The original single-diode model of a single PV cell is depicted in Fig. 1.

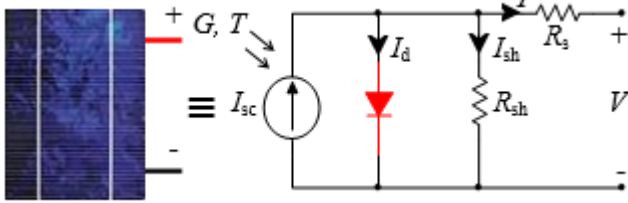


Figure 1. Single-diode model of a PV cell

The source of nonlinearity in an original PV model is the diode. Where the diode's current-voltage relationship is described by the following exponential form [19]:

$$I_d = I_o(\exp((q \cdot V_d)/(N_s \cdot a \cdot K \cdot T)) - 1), \quad (1)$$

$$V_d = V + I \cdot R_s \quad (2)$$

Where I_d and V_d are the diode's current and voltage, respectively; I_o is the diode's reverse current; and R_s is the series resistance. Meanwhile, I and V are the module's current and voltage, respectively.

This article uses a piecewise method to linearize the diode's nonlinear I-V characteristic [17]-[18]. The PV single-diode model is linearized, as depicted in Fig. 2. This method can be summarized by splitting the original nonlinear curve into several sections. In each section, a straight line between two linearization points is utilized, to substitute the original nonlinear curve, as depicts in Fig. 2. In this figure, the original characteristic of the diode is split into three sections, each one is defined by a linear straight line and two linearization point at the boundaries. The number of linearization points is usually more than the number of sections by one. Hence, the number of points is four, and each point is defined by a diode's voltage and current (V_d , I_d), as shown in Fig. 2. The straight line of each section can be represented electrically by a source of voltage (V_{dx}) and diode resistance (R_d). V_{dx} represents the intersection

value of the straight line across the voltage x-axis in each section. R_d represents the reciprocal of the straight line's slope in each section.

In Fig. 2, three voltage sources are denoted by V_{dx1} , V_{dx2} , and V_{dx3} . In contrast, three diode resistances are denoted by R_{d1} , R_{d2} , and R_{d3} .

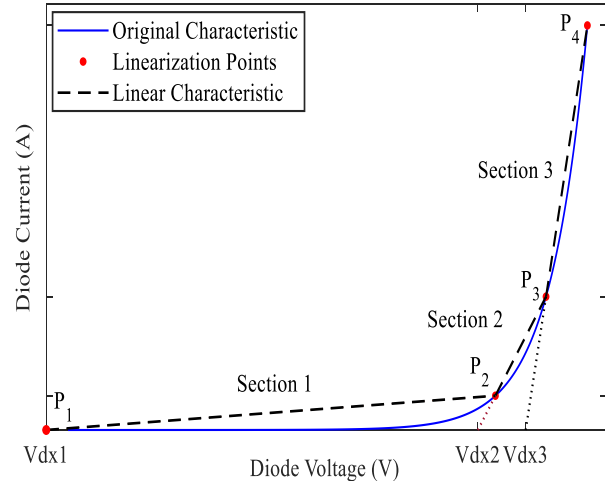


Figure 2. I-V characteristic of the diode

Fig. 2 clearly shows an evident error between the original nonlinear and a linearized diode's characteristics in all operating points except the linearized points. At the linearized points, the error is zero.

After linearization, the linearized single-diode model can be depicted in Fig. 3.

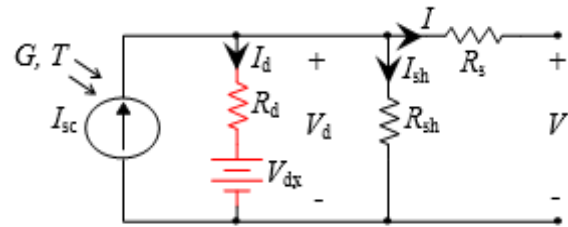


Figure 3. Linearized PV single-diode model

According to the circuit shown in Fig. 3, the Thevenin equivalent circuit of the PV can be derived. Firstly, by solving (3) and (4):

$$V_{dxj} + I_{dj} \cdot R_{dj} - I_{shj} \cdot R_{sh} = 0, \quad (3)$$

$$I_{shj} = I_{sc} - I_{dj} \quad (4)$$

I_{dj} and I_{shj} can result in:

$$I_{dj} = (I_{sc} \cdot R_{sh} - V_{dxj}) / (R_{sh} + R_{dj}), \quad (5)$$

$$I_{shj} = (V_{dxj} + I_{sc} \cdot R_{dj}) / (R_{sh} + R_{dj}) \quad (6)$$

R_{sh} is a parallel resistance, and j is the instantaneous section number. Hence, V_{th} can be derived as:

$$V_{thj} = I_{shj} \cdot R_{sh}, \quad (7)$$

$$\therefore V_{thj} = (V_{dxj} + I_{sc} \cdot R_{dj}) \cdot R_{sh} / (R_{sh} + R_{dj}) \quad (8)$$

R_{th} can be derived by opening the current source, shorting the voltage source, then calculating the equivalent resistance through the output terminals of the circuit shown in Fig. 3. Consequently, R_{th} can be presented as:

$$R_{thj} = R_s + \frac{R_{sh} \times R_{dj}}{R_{sh} + R_{dj}} \quad (9)$$

Since the amounts of V_{dxj} and R_{dj} are dependent on the instantaneous section number (j) of the PV operating point, the amounts of V_{thj} and R_{thj} are also dependent on the section number (j) as shown in (8) and (9), respectively. After all, the resultant Thevenin equivalent circuit for the circuit depicted in Fig. 3 is illustrated in Fig. 4.

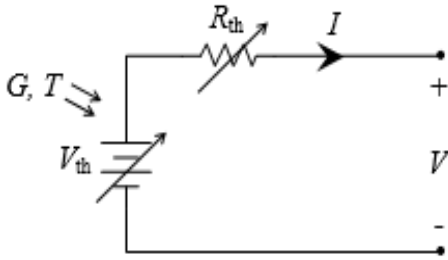


Figure 4. PV Thevenin equivalent circuit

In a PV system, a maximum power point tracker (MPPT) is typically used to track the MPP of the PV panel in order to harvest the maximum amount of power available under different operating conditions [15],[19]-[22]. Hence, because of the MPP's importance, this point is selected as one of the linearized points in the linearization method. At this point, the error is zero. Other linearized points are selected so that the error is as minimal as possible.

3. Characteristics of the PV Module

Its I-V and P-V characteristics can represent the characteristics of any PV. The original nonlinear I-V characteristic of the single-diode model depicted in Fig. 1 can be illustrated by [19]:

$$I = I_{sc} - I_d - (V + I \cdot R_s)/R_{sh} \quad (10)$$

From (10), it is clear that a numerical iterative method is needed to calculate I for each given value of V .

In this article, the BP SX150S PV module is chosen. This module comprises 72 series cells ($N_s=72$), which provide an MPP power of 150 W under standard technical conditions (STC).

The remaining main specifications of this module under STC are: open-circuit voltage (V_{oc}) of 43.5 V, short-circuit current (I_{sc}) of 4.75 A, and MPP's voltage and current of 34.5 V and 4.35 A, respectively [23]. In contrast, the I-V characteristic of the PV Thevenin equivalent circuit shown in Fig. 4 can be represented at each operating section (j) by:

$$I = \frac{V_{thj} - V}{R_{thj}} \quad (11)$$

For each section (j) and by using (1) and (2), the diode's voltage and current at the boundaries of a linear straight line which are defined by (V_{d1}, I_{d1}) and (V_{d2}, I_{d2}) can be calculated. Accordingly, the values of R_{dj} and V_{dxj} can be calculated as:

$$R_d = \frac{V_{d2} - V_{d1}}{I_{d2} - I_{d1}}, \quad (12)$$

$$V_{dx} = V_{d1} - R_d \cdot I_{d1} = V_{d2} - R_d \cdot I_{d2} \quad (13)$$

Now, V_{th} and R_{th} can be easily calculated by substituting the values of V_{dx} and R_d in (8) and (9). Subsequently, using (11), I can calculate directly for each value of V without needing the numerical iterative method. About the P-V characteristic, it can be easily obtained for each operating point by:

$$P = I \cdot V \quad (14)$$

4. Results and Discussions

In this article, the characteristics of the BP SX150S PV module based on the proposed Thevenin's equivalent circuit are evaluated and compared with those of the original PV model under three scenarios of irradiance (G) and temperature (T) conditions for a voltage range from 0 to V_{oc} .

In the first scenario, the weather condition is STC ($G=1000$ W/m² and $T=25$ °C). In the second scenario, the irradiance is decreased from 1000 W/m² to 400 W/m² while the temperature is kept at 25 °C; hence, the condition is defined as $G=400$ W/m² and $T=25$ °C. In the third suggested scenario, the irradiance is kept at 1000 W/m² while the temperature is increased to 50 °C; hence, the condition is defined as $G=1000$ W/m² and $T=50$ °C. The linearization method selects 12 points (P_1, P_2, \dots, P_{12}) to linearize the diode's characteristic. Hence, 11 sections of different values of V_{th} and R_{th} are produced. The first (P_1) and last (P_{12}) points are selected at the short-circuit and open-circuit voltages, respectively. The MPP is also selected as P_4 due to its importance. According to the remaining 9 points, two points (P_2 and P_3) are distributed uniformly on the left side of the MPP, while the seven points (P_5, P_6, \dots, P_{11}) are distributed uniformly on the right side of the MPP. In this work, most of the points are concentrated on the right side because the diode's characteristic is inherently nonlinear on this side.

To examine the activity of the proposed model under different operating conditions, the error of the Thevenin's characteristics related to the original characteristics is calculated. The error can be defined as:

$$\text{error (\%)} = (I_{orig} - I_{thev})/I_{orig} \times 100 \quad (15)$$

Where I_{orig} is the current of the PV module based on the original PV nonlinear model, and I_{thev} is the current of the PV module based on the proposed Thevenin's equivalent circuit.

In the first scenario, Fig. 5 shows the PV module's I-V and corresponding P-V characteristics based on both the original and Thevenin's models. Furthermore, Fig. 6 illustrates the error (in percentage).

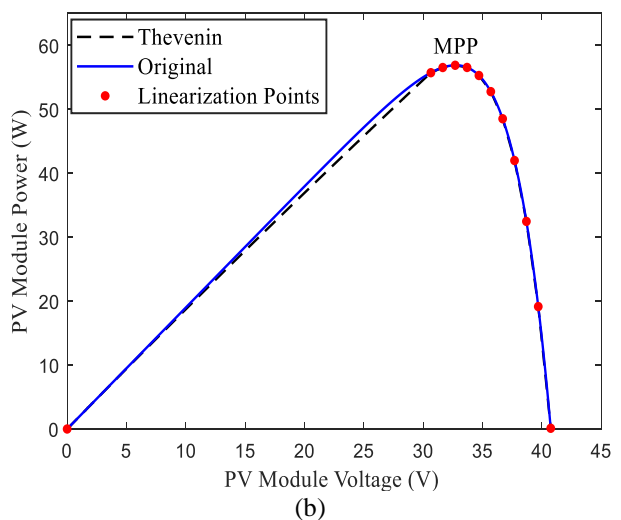
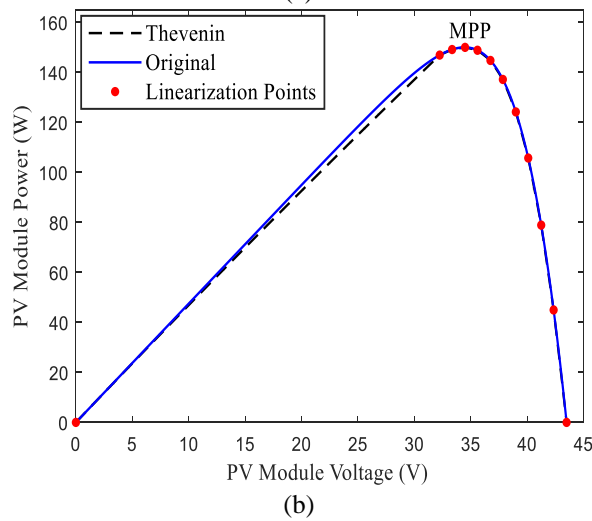
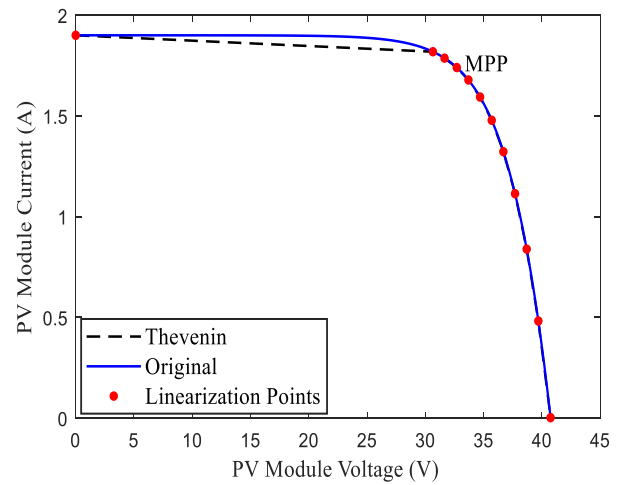
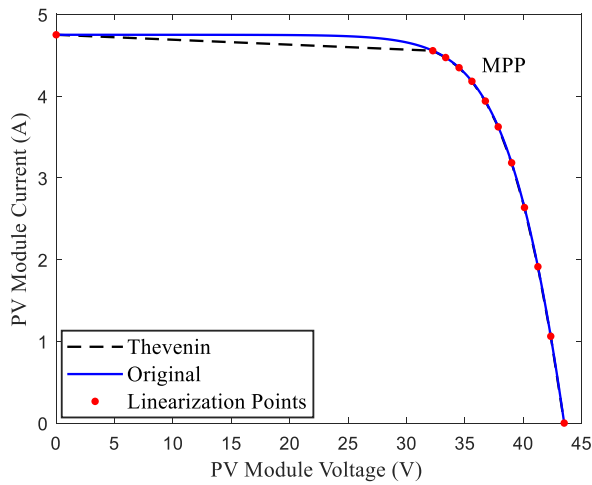


Figure 5. PV module characteristics based on original and Thevenin's models at STC: (a) *I-V* curves; (b) *P-V* curves

Figure 7. PV module characteristics based on original and Thevenin's models at 400 W/m² and 25 °C: (a) *I-V* curves; (b) *P-V* curves

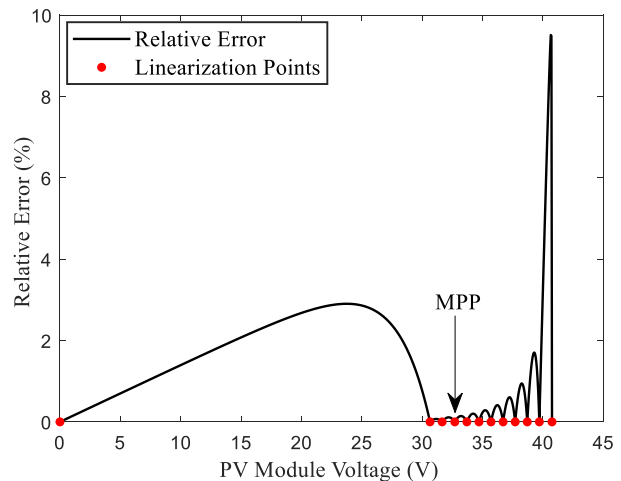
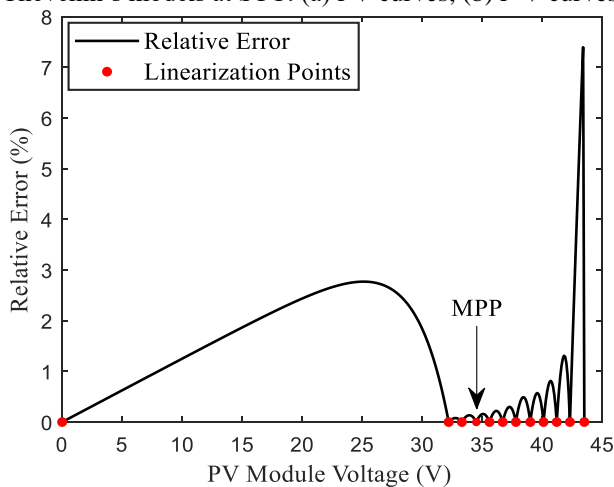


Figure 6. Error in characteristics between the original and the Thevenin's models at STC

Figure 8. Error in characteristics between original and Thevenin's models at 400 W/m² and 25 °C

In the second scenario, Fig. 7 displays the *I-V* and *P-V* characteristics of the PV module based on both the original and Thevenin's models. In addition, Fig. 8 shows the error (as a percentage).

In the third scenario, Fig. 9 shows the PV modules' *I-V* and *P-V* characteristics based on both the original and Thevenin's models. Additionally, Fig. 10 displays the error (as a percentage).

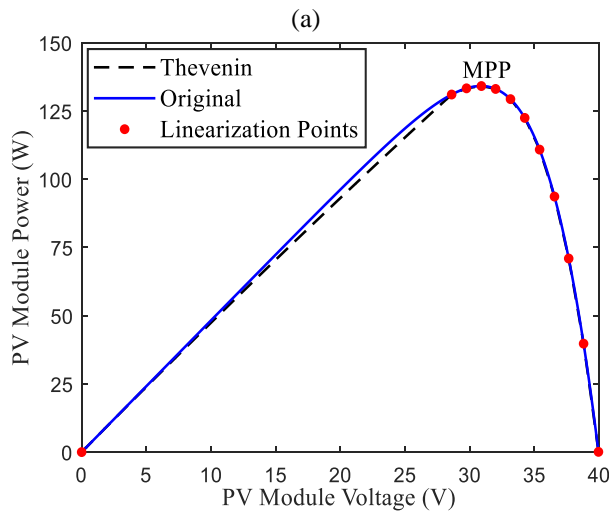
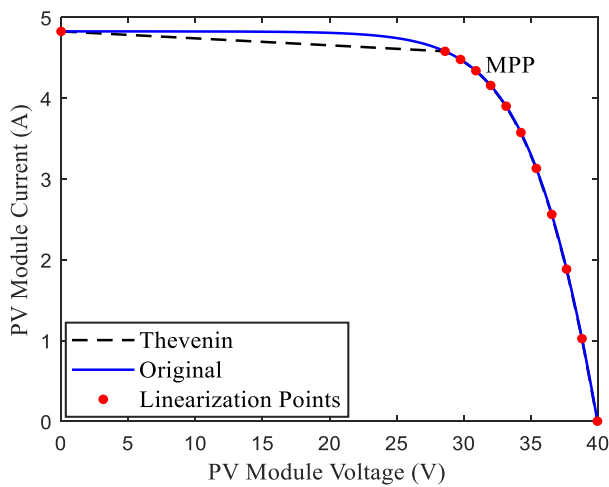


Figure 9. PV module characteristics based on original and Thevenin’s models at 1000 W/m² and 50 °C: (a) *I-V* curves; (b) *P-V* curves

Table 1. Parameters of linearization and the Thevenin equivalent circuit at STC

Module Voltage (V)	V_{d1}, I_{d1}	V_{d2}, I_{d2}	V_{dx} (V)	R_d (Ω)	V_{th} (V)	R_{th} (Ω)
0 – 32.25	0.0244, 0	32.2734, 0.1948	0.0241	165.5819	786.5383	165.5871
32.25 – 33.35	32.2734, 0.1948	33.3729, 0.2783	29.7100	13.1614	92.2267	13.1665
33.35 – 34.50	33.3729, 0.2783	34.5223, 0.4024	30.7945	9.2645	74.8011	9.2697
34.50 – 35.60	34.5223, 0.4024	35.6215, 0.5691	31.8697	6.5924	63.1836	6.5975
35.60 – 36.75	35.6215, 0.5691	36.7702, 0.8109	32.9180	4.7505	55.4827	4.7556
36.75 – 37.85	36.7702, 0.8109	37.8686, 1.1261	33.9444	3.4846	50.4965	3.4898
37.85 – 39.00	37.8686, 1.1261	39.0163, 1.5659	34.9298	2.6097	47.3257	2.6148
39.00 – 40.10	39.0163, 1.5659	40.1135, 2.1132	35.8771	2.0047	45.3994	2.0098
40.10 – 41.25	40.1135, 2.1132	41.2598, 2.8373	36.7681	1.5831	44.2878	1.5882
41.25 – 42.35	41.2598, 2.8373	42.3554, 3.6883	37.6066	1.2876	43.7225	1.2927
42.35 – 43.50	42.3554, 3.6883	43.5000, 4.7500	38.3795	1.0780	43.5000	1.0831

Table 2. Parameters of linearization and the Thevenin equivalent circuit at 400 W/m² and 25 °C

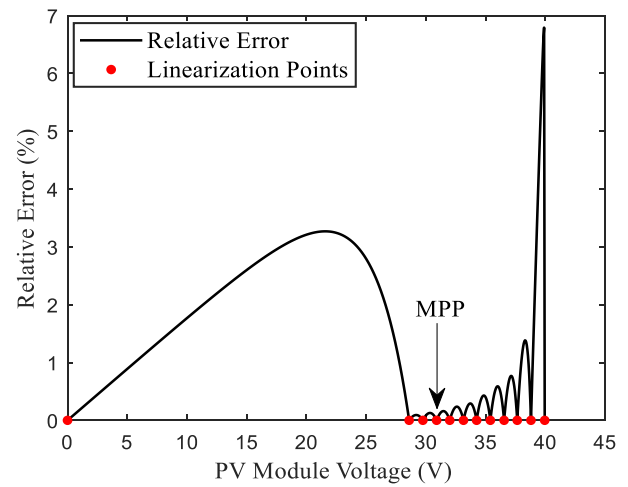


Figure 10. Error in characteristics between original and Thevenin’s models at 1000 W/m² and 50 °C

Tables 1, 2, and 3 state the calculated values of V_{d1} , I_{d1} , V_{d2} , I_{d2} , V_{dx} , R_d , V_{th} , and R_{th} at the various module voltages within each operating section based on the proposed Thevenin model. The values of module voltage at the MPP are 34.5 V, 32.7 V, and 30.9 V under the conditions of scenario 1, scenario 2, and scenario 3, respectively.

Tables 1, 2, and 3 illustrate that increasing the module voltage decreases the values of V_{th} and R_{th} due to decreasing R_d .

Under the different weather conditions, Fig. 5 through Fig. 10 show that the characteristics of the PV module based on both the original and Thevenin’s models are fairly similar. Moreover, the error is zero at the linearized points, which include the MPP.

Module Voltage (V)	V_{d1}, I_{d1}	V_{d2}, I_{d2}	V_{dx} (V)	R_d (Ω)	V_{th} (V)	R_{th} (Ω)
0 – 30.65	0.0097, 0	30.6593, 0.0815	0.0095	376.2714	714.9251	376.2765
30.65 – 31.65	30.6593, 0.0815	31.6592, 0.1133	28.1014	31.4017	87.7648	31.4069
31.65 – 32.70	31.6592, 0.1133	32.7089, 0.1599	29.1094	22.5049	71.8687	22.5100
32.70 – 33.70	32.7089, 0.1599	33.7086, 0.2216	30.1175	16.2022	60.9017	16.2073
33.70 – 34.70	33.7086, 0.2216	34.7082, 0.3063	31.0909	11.8104	53.5306	11.8155
34.70 – 35.70	34.7082, 0.3063	35.7076, 0.4216	32.0546	8.6640	48.5162	8.6691
35.70 – 36.70	35.7076, 0.4216	36.7068, 0.5775	33.0053	6.4092	45.1828	6.4144
36.70 – 37.70	36.7068, 0.5775	37.7057, 0.7860	33.9390	4.7925	43.0447	4.7976
37.70 – 38.70	37.7057, 0.7860	38.7043, 1.0609	34.8509	3.6322	41.7521	3.6373
38.70 – 39.70	38.7043, 1.0609	39.7025, 1.4176	35.7357	2.7982	41.0523	2.8033
39.70 – 40.75	39.7025, 1.4176	40.7500, 1.8972	36.6060	2.1843	40.7561	2.1894

Table 3. Parameters of linearization and the Thevenin equivalent circuit at 1000 W/m² and 50 °C

Module Voltage (V)	V_{d1}, I_{d1}	V_{d2}, I_{d2}	V_{dx} (V)	R_d (Ω)	V_{th} (V)	R_{th} (Ω)
0 – 28.60	0.0248, 0	28.6235, 0.2463	0.0229	116.1289	560.5987	116.1340
28.60 – 29.75	28.6235, 0.2463	29.7730, 0.3470	25.8121	11.4151	80.9152	11.4203
29.75 – 30.90	29.7730, 0.3470	30.9223, 0.4867	26.9185	8.2267	66.6302	8.2318
30.90 – 32.00	30.9223, 0.4867	32.0213, 0.6689	27.9876	6.0300	57.0957	6.0352
32.00 – 33.15	32.0213, 0.6689	33.1700, 0.9258	29.0302	4.4714	50.6145	4.4765
33.15 – 34.25	33.1700, 0.9258	34.2683, 1.2519	30.0514	3.3684	46.3112	3.3735
34.25 – 35.40	34.2683, 1.2519	35.4161, 1.6961	31.0338	2.5837	43.5056	2.5888
35.40 – 36.55	35.4161, 1.6961	36.5631, 2.2655	31.9989	2.0147	41.7242	2.0198
36.55 – 37.65	36.5631, 2.2655	37.6597, 2.9432	32.8976	1.6180	40.7079	1.6231
37.65 – 38.80	37.6597, 2.9432	38.8053, 3.8033	33.7393	1.3320	40.1691	1.3371
38.80 – 39.95	38.8053, 3.8033	39.9500, 4.8250	34.5442	1.1204	39.9524	1.1255

In contrast, the errors are observed on the other points and reach peak values near the V_{oc} , under the conditions of scenario 1, scenario 2, and scenario 3, as demonstrated in Figs. 6, 8, and 10, respectively. The peak values are approximately 7.37%, 9.51%, and 6.79% at module voltages of 43.45 V, 40.65 V, and 39.9 V, respectively. Nevertheless, the error distribution is larger on the left side of the MPP than on the right due to the lower number of selected linearized points on this side, as depicted in Figs. 6, 8, and 10. The values of the integral of squared error (ISE) on the left side are 0.257, 0.042, and 0.325, while those values do not exceed 0.0013, 0.0003, and 0.0011 on the right side of Figs. 6, 8, and 10, respectively.

5. Conclusions

It is concluded from the simulation results that the Thevenin's equivalent circuit can successfully model the PV module. The PV characteristics based on the proposed Thevenin model are similar to the original characteristics based on the single-diode model, especially on the MPP and linearized point, as depicted in Figs. 5, 7, and 9. Moreover, the effectiveness of the proposed model is increased by increasing the number of points selected in the linearization. The error is minimal on the right of MPP under different weather conditions, as illustrated in Figs. 6, 8, and 10.

In this work, except for the short-circuit and open-circuit voltage points, seven selected points are uniformly distributed on the right of MPP, representing a much nonlinear region. Whereas, only two selected points are distributed on the left of MPP. Despite the large distribution for linearized points on the right of MPP, it is seen that the peak value of the error exists there, as demonstrated in Figs. 6, 8, and 10. Hence, for PV applications requiring a module working at the right side of the MPP (i.e., $V > V_{load}$), more points have to be distributed on this side to decrease the linearization error as much as possible. In conclusion, the proposed model can be successfully used to study the performance of PV systems under different conditions, avoiding the numerical iterative solutions for nonlinear equations of the original PV model. For future work, the proposed PV model can be integrated with a converter/inverter and load to study a PV system's performance and confirm that MPPT is operating correctly, under different operating conditions.

Acknowledgements

The authors would like to express their appreciation to Mustansiriyah University (www.uomustansiriyah.edu.iq), Baghdad-Iraq, for its assistance and academic advice in completing this work.

Conflict of interest

The authors declare that there are no conflicts of interest regarding the publication of this article.

Author Contribution Statement

Ammar Al-Gizi and Abbas Hussien Miry proposed the research problem.

Ammar Al-Gizi and Hussein M. Hathal developed the theory and carried out the calculations.

Ammar Al-Gizi and Aurelian Craciunescu evaluated and compared the characteristics of the BP SX150S PV module based on the proposed Thevenin's equivalent circuit with those of the original PV model under three scenarios of irradiance (G) and temperature (T) conditions.

All authors analyzed the findings and participated in the final article.

References

- [1] M. Mohamed Nazief Haggag Kotb Kholaf, M. Xiao, and X. Tang, "COVID-19's fear-uncertainty effect on renewable energy supply chain management and ecological sustainability performance; the moderate effect of big-data analytics," *Sustain. Energy Technol. Assess.*, vol. 53, p. 102622, Oct. 2022, doi: <https://doi.org/10.1016/j.seta.2022.102622>.
- [2] B. Steffen and A. Patt, "A historical turning point? Early evidence on how the Russia-Ukraine war changes public support for clean energy policies," *Energy Res. & Soc. Sci.*, vol. 91, p. 102758, Sept. 2022, doi: <https://doi.org/10.1016/j.erss.2022.102758>.
- [3] G. Li, G. Li, and M. Zhou, "Model and application of renewable energy accommodation capacity calculation considering utilization level of interprovincial tie-line," *Prot. Control Mod.. Power Syst.*, vol. 4, no. 1, pp. 1-12, Jan. 2019, doi: <https://doi.org/10.1186/s41601-019-0115-7>.
- [4] M. C. Pamponet, H. L. Maranduba, J. A. de Almeida Neto, and L. B. Rodrigues, "Energy balance and carbon footprint of very largescale photovoltaic power plant," *Int. J. Energy Res.*, vol. 46, no. 5, pp. 6901-6918, 2022, doi: <https://doi.org/10.1002/er.7529>.
- [5] B. Li *et al.*, "Modeling Integrated Power and Transportation Systems: Impacts of Power-to-Gas on the Deep Decarbonization," *IEEE Trans. Ind. Appl.*, vol. 58, no. 2, pp. 2677-2693, Mar. 2022, doi: <https://doi.org/10.1109/TIA.2021.3116916>.
- [6] M. Drif, M. Bahri, and D. Saigaa, "A novel equivalent circuit-based model for photovoltaic sources," *Optik*, vol. 242, p. 167046, Sept. 2021, doi: <https://doi.org/10.1016/j.ijleo.2021.167046>.
- [7] J. Warmke, *Understanding Photovoltaics: Designing and Installing Residential Solar Systems*. 8th ed., Virginia Ridge Road, Philo, OH, USA: Blue Rock Station LLC, Oct. 2020.
- [8] S. K. Goyal, B. P. Sungh, A. Kumar, P. Kumar, and A. Saraswat, "Modelling and simulation of a solar PV system: a comprehensive study," in *2020 International Conference on Computation, Automation and Knowledge Management (ICCAKM)*, Dubai, United Arab Emirates, 2020, pp. 367-372, doi: <https://doi.org/10.1109/ICCAKM46823.2020.9051497>.
- [9] F. E. Ndi, S. N. Perabi, S. E. Ndjakomo, G. O. Abessolo, and G. M. Mengata, "Estimation of single-diode and two diode solar cell parameters by equilibrium optimizer method," *Energy Reports*, vol. 7, pp. 4761-4768, Nov. 2021, doi: <https://doi.org/10.1016/j.egyrs.2021.07.025>.
- [10] D. H. Muhsen, H. T. Haider, and H. I. Shahadi, "Parameter extraction of single-diode PV-module model using electromagnetism-like algorithm," *Journal of Engineering and Sustainable Development*, vol. 22, no. 2 (part 2), pp. 161-172, Mar. 2018, doi: <https://doi.org/10.31272/jeasd.2018.2.26>.
- [11] S. Yu., A. A. Heidari, G. Liang, C. Chen, H. Chen, and Q. Shao, "Solar photovoltaic model parameter estimation based on orthogonally-adapted gradient-based optimization," *Optik*, vol. 252, p. 168513, Feb. 2022, doi: <https://doi.org/10.1016/j.ijleo.2021.168513>.
- [12] E. Rodrigues, R. Melicio, V. Mendes, and J.P. Catalao, "Simulation of a solar cell considering single-diode equivalent circuit model," *Renewable Energy & Power Quality Journal*, vol. 1, no. 9, pp. 369-373, May 2011, doi: <https://doi.org/10.24084/repqj09.339>.
- [13] M. M. Abbas, and D. H. Muhsen, "Extraction of double-diode photovoltaic module model's parameters using hybrid optimization algorithm," *Journal of Engineering and Sustainable Development*, vol. 26, no. 4, pp. 77-91, Jul. 2022, doi: <https://doi.org/10.31272/jeasd.26.4.9>.
- [14] L. Bouhaki, R. Saadani, and M. Rahmoune, "Comparison between single-diode and two diodes of a grid connected PV technologies: numerical study and experimental validation," *Int. J. Power Electron. Drive Syst.*, vol. 11, no. 2, pp. 914-920, Jun. 2020, doi: <https://doi.org/10.11591/ijpeds.v11.i2.pp914-920>.
- [15] A. Al-Gizi, A. H. Miry, and M. A. Shehab, "Optimization of fuzzy photovoltaic maximum power point tracking controller using chimp algorithm," *Int. J. Electr. Comput. Eng.*, vol. 12, no. 5, pp. 4549-4558, Oct. 2022, doi: <https://doi.org/10.11591/ijece.v12i5.pp4549-4558>.
- [16] C. Osigwe, "Thevenin Equivalent of Solar Cell Model," Master's thesis, Minnesota State University, Mankato, 2019. Available: <https://cornerstone.lib.mnsu.edu/etds/971/>
- [17] M.-H. Lin, J. G. Carlsson, D. Ge, J. Shi, and J.-F. Tsai, "A review of piecewise linearization methods," *Mathematical Problems in Engineering*, vol. 2013, no. 1, p. 101376, Nov. 2013, doi: <https://doi.org/10.1155/2013/101376>.
- [18] M. Asghari, A. M. Fathollahi-Fard, S. Mirzapour Al-E-Hashem, and M.A. Dulebenets, "Transformation and linearization techniques in optimization: A state-of-the-art survey," *Mathematics*, vol. 10, no. 2, p. 283, Jan. 2022, doi: <https://doi.org/10.3390/math10020283>.
- [19] A. Al-Gizi, S. Al-Chlahawi, M. Louzazni, and A. Craciunescu, "Genetically optimization of an asymmetrical fuzzy logic based photovoltaic maximum power point tracking controller," *Adv. Electr. Comput. Eng.*, vol. 17, no. 4, pp. 69-76, Nov. 2017, doi: <https://doi.org/10.4316/aecce.2017.04009>.
- [20] R. H. Ahmed, S. H. Rhaif, and S. A. Hashem, "Fuzzy logic control to process change irradiation and temperature in the solar cell by controlling for maximum power point," *Journal of Engineering and Sustainable Development*, vol. 27, no. 1, pp. 28-36, Jan. 2023, doi: <https://doi.org/10.31272/jeasd.27.1.3>.
- [21] N. Van Tan, N. B. Nam, N. H. Hieu, L. K. Hung, M. Q. Duong, and L. H. Lam, "A proposal for an MPPT algorithm based on the fluctuations of the PV output power, output voltage, and control duty cycle for improving the performance of PV systems in microgrid," *Energies*, vol. 13, no. 17, p. 4326, Aug. 2020, doi: <https://doi.org/10.3390/en13174326>.
- [22] A. Al-Gizi, A. H. Miry, H. M. Hathal, and A. Craciunescu, "Fuzzy maximum power point tracking controllers for photovoltaic systems: a comparative analysis," *Journal of Engineering and Sustainable Development*, vol. 28, no. 3, pp. 364-374, May 2024, doi: <https://doi.org/10.31272/jeasd.28.3.6>.
- [23] Bpsolar. "Proven Materials and Construction Quality and Safety BP SX 150S TÜV Clear-Anodized Universal Frame DC Connectors." Accessed: Jan. 25, 2025. [Online]. Available: <https://www.abc-solar.com/pdf/bpsx150.pdf>